PAPER

Symmetries of the squeeze-driven Kerr oscillator

IOP Publishing Journal of Physics A: Mathematical and Theoretical
J. Phys. A: Math. Theor. **56** (2023) 495305 (25pp) https://doi.org/10.1088/1751-8121/ad09eb

Symmetries of the squeeze-driven Kerr oscillator

Francesco Iachello[1], Rodrigo G Cortiñas[2], Francisco Pérez-Bernal[3,4,*] and Lea F Santos[5]

[1] Center for Theoretical Physics, Sloane Physics Laboratory, Yale University, New Haven, CT 06520-8120, United States of America
[2] Yale Quantum Institute, Department of Applied Physics and Physics, Yale University, New Haven, CT 06520, United States of America
[3] Depto. de Ciencias Integradas y Centro de Estudios Avanzados en Física, Matemáticas y Computación, Universidad de Huelva, Huelva 21071, Spain
[4] Instituto Carlos I de Física Teórica y Computacional, Universidad de Granada, Fuentenueva s/n, 18071 Granada, Spain
[5] Department of Physics, University of Connecticut, Storrs, CT 06269, United States of America

E-mail: francisco.perez@dfaie.uhu.es

Received 5 June 2023; revised 16 October 2023
Accepted for publication 6 November 2023
Published 20 November 2023

Abstract

We study the symmetries of the static effective Hamiltonian of a driven superconducting nonlinear oscillator, the so-called squeeze-driven Kerr Hamiltonian, and discover a remarkable quasi-spin symmetry $su(2)$ at integer values of the ratio $\eta = \Delta/K$ of the detuning parameter Δ to the Kerr coefficient K. We investigate the stability of this newly discovered symmetry to high-order perturbations arising from the static effective expansion of the driven Hamiltonian. Our finding may find applications in the generation and stabilization of states useful for quantum computing. Finally, we discuss other Hamiltonians with similar properties and within reach of current technologies.

Keywords: Kerr parametric oscillator, squeeze-driven Kerr oscillator, local symmetry, quasi-spin symmetry, excited-state quantum phase transition

(Some figures may appear in colour only in the online journal)

* Author to whom any correspondence should be addressed.

1. Introduction

Kerr-nonlinear parametric oscillators (KPOs) have been suggested as devices for quantum computation [1, 2]. A KPO can generate Schrödinger cat states via quantum adiabatic evolution through its bifurcation point. These states correspond to quantum superpositions of coherent states and they are protected against photon dephasing errors, which has motivated their use as the logical states of a qubit [3]. A considerable amount of effort has gone in the last few years in developing KPOs that can generate cat states deterministically, especially with superconducting circuits with Josephson junctions [4–11]. In these circuits, the non-linearity of the Josephson junctions is used for achieving large Kerr effects [12–16] and the magnetic flux of a superconducting quantum interference device (SQUID) is used for the parametric modulation [17–23].

Theoretical studies [24–32] have inspired the analysis of the results of several experimental implementations of single KPOs [8–10]. A useful tool for these studies is the conversion of the time-dependent Hamiltonian describing the experimental system into a static effective Hamiltonian. Recently, a general method for this conversion has been developed [9, 11, 33, 34], wherein the static effective Hamiltonian is obtained as a boson expansion in terms of one-dimensional boson annihilation and creation operators, $\hat{a}$ and $\hat{a}^\dagger$, with $[\hat{a}, \hat{a}^\dagger] = 1$. To second order in the boson expansion, the static effective Hamiltonian of a driven superconducting nonlinear (Kerr) oscillator in the quantum regime was obtained as [9, 10],

$$\hat{H} = -\Delta \hat{a}^\dagger \hat{a} + K \hat{a}^{\dagger 2} \hat{a}^2 - \varepsilon_2 \left(\hat{a}^{\dagger 2} + \hat{a}^2 \right), \tag{1}$$

where the detuning Δ, the Kerr coefficient K, and the squeezing amplitude ε_2 are explicit functions of the parameters of a driven quantum circuit. We note that, for convenience, Hamiltonian (1) differs from that in [9, 10] by an overall minus sign. This change in sign was also made in [2] to conform with standard quantum computing notation.

The spectrum of the driven system was experimentally measured as a function of the control parameters Δ, K, and ε_2 [9] and was found to be accurately described by the second-order Hamiltonian (1), although deviations may occur for large nonlinearities [35]. The observed spectrum shows remarkable properties for integer values of the ratio $\eta = \Delta/K$, which persist even when the squeezing amplitude is increased to non-perturbative values [10]. Specifically, the spectrum presents real crossings when η is even and avoided crossings when η is odd [10], which implies that by tuning the parameters of the system, one can suppress or enhance quantum tunneling [10, 36]. The spectrum also exhibits an excited state quantum phase transition (ESQPT) as a function of the squeezing amplitude ε_2 [36, 37]. This ESQPT is similar to the QPTs observed in other systems, such as driven Rabi and Dicke models [38, 39] and the Jaynes–Cummings model [38].

In this article, we uncover the symmetries of the squeeze-driven Kerr oscillator, in particular, the one that occurs as a function of Δ and which may play an important role in the generation of stable states for quantum computing [10, 40]. The symmetry, which occurs for integer values of the dimensionless parameter $\eta = \Delta/K$, is a dynamic symmetry [41] similar to those observed in the interacting boson model of nuclear physics [42] and the vibron model of molecular physics [43]. Dynamic symmetries are situations in which the eigenvalues of $\hat{H}$ can be written in terms of quantum numbers labelling the irreducible representations of an algebra $g \supset g' \supset \ldots$ and often display degeneracies associated with the subalgebras $g' \supset \ldots$ of g [44]. They have played a major role in the analysis of data in a variety of fields, including

molecular, atomic, nuclear, and particle physics. The symmetry which occurs for integer values of $\eta = \Delta/K$ can also be labelled a 'local' symmetry, since it occurs for special values in the parameter space. It differs from the 'global' symmetry parity, $\Pi \equiv Z_2$, of the Hamiltonian of the squeeze-driven Kerr oscillator (1), which occurs for any value in the parameter space. (The global Z_2 symmetry of the Kerr oscillator (1) and of similar models has been investigated by many authors, especially in connection with the Limbladian operator obtained from the Hamiltonian operator [45, 46].)

After the identification in sections 2 and 3 of the spectrum generating algebra of the problem as the symplectic algebra $sp(2,\mathbb{R})$ and of its alternative Heisenberg algebra $h(2)$, we introduce, in section 4.1, the novel and unexpected quasi-spin symmetry $su(2)$ of the Kerr oscillator $\hat{H} = -\Delta\hat{a}^\dagger\hat{a} + K\hat{a}^{\dagger^2}\hat{a}^2$. We then return to the squeeze-driven Kerr oscillator of (1) and discuss, in sections 4.2 and 4.3, its relationship with the theory of ESQPTs [47–49]. In section 5, we discuss other Hamiltonians with similar properties and within the reach of current technologies. Conclusions are presented in section 6.

2. Algebraic structure of the squeeze-driven Kerr oscillator

To reveal the symmetries of the squeeze-driven Kerr Hamiltonian [9, 10], we rewrite Hamiltonian (1) as

$$\hat{H} = -\Delta\left(\hat{a}^\dagger\hat{a}\right) + K\left(\hat{a}^\dagger\hat{a}\right)\left(\hat{a}^\dagger\hat{a} - 1\right) - \varepsilon_2\left(\hat{a}^\dagger\hat{a}^\dagger + \hat{a}\hat{a}\right), \tag{2}$$

or, in short,

$$\hat{H} = -\Delta\hat{n} + K\hat{n}\left(\hat{n} - 1\right) - \varepsilon_2\hat{P}_2, \tag{3}$$

where $\hat{n} = \hat{a}^\dagger\hat{a}$ is the number operator and $\hat{P}_2 = \hat{a}^\dagger\hat{a}^\dagger + \hat{a}\hat{a}$ is the pairing operator of order two.

The three operators in (2),

$$\hat{F}_+ = \hat{a}^\dagger\hat{a}^\dagger\ ,\ \ \hat{F}_- = \hat{a}\hat{a}\ ,\ \ \hat{F}_z = \hat{a}^\dagger\hat{a}, \tag{4}$$

form a closed algebra with commutation relations

$$\left[\hat{F}_z, \hat{F}_\pm\right] = \pm 2\hat{F}_\pm\ ,\ \ \left[\hat{F}_+, \hat{F}_-\right] = -4\hat{F}_z - 2. \tag{5}$$

This algebra is the symplectic algebra $sp(2,\mathbb{R})$ [50]. The algebra $sp(2,\mathbb{R})$ is isomorphic to $su(1,1)$, the non-compact version of $su(2)$ [44], as one can see by considering the operators

$$\hat{F}_+^{''} = \frac{1}{2}\left(\hat{a}^\dagger\hat{a}^\dagger\right)\ ,\ \ \hat{F}_-^{''} = \frac{1}{2}\left(\hat{a}\hat{a}\right)\ ,\ \ \hat{F}_z^{''} = \frac{1}{2}\left(\hat{a}^\dagger\hat{a} + \frac{1}{2}\right), \tag{6}$$

satisfying the standard form of the commutation relations of $su(1,1)$

$$\left[\hat{F}_z^{''}, \hat{F}_\pm^{''}\right] = \pm\hat{F}_\pm^{''}\ ,\ \ \left[\hat{F}_+^{''}, \hat{F}_-^{''}\right] = -2\hat{F}_z^{''}. \tag{7}$$

Since the Hamiltonian is written in terms of elements of this algebra,

$$\hat{H} = -\Delta\hat{F}_z + K\hat{F}_z\left(\hat{F}_z - 1\right) - \varepsilon_2\left(\hat{F}_+ + \hat{F}_-\right), \tag{8}$$

$sp(2,\mathbb{R})$ is the spectrum generating algebra [41] of the Kerr problem at first and second orders. Also, introducing $\hat{F}_\pm = \hat{F}_x \pm i\hat{F}_y$, the last term can be written as $\hat{F}_+ + \hat{F}_- = 2\hat{F}_x$.

The boson expansion of the effective Hamiltonian of a squeeze-driven Kerr oscillator was carried out to orders three and four in [9], since these terms can also be experimentally implemented with the appropriate choice of the parameters in the time-dependent Hamiltonian. At third order, the additional contributions to the effective Hamiltonian can be written as [9, 10]

$$\hat{H}^{(3)} = -\Delta^{(3)}\left(\hat{a}^\dagger\hat{a}\right) - K^{(3)}\left(\hat{a}^\dagger\hat{a}\right)\left(\hat{a}^\dagger\hat{a}-1\right) + \varepsilon_2^{(3)}\left(\hat{a}^{\dagger 2}+\hat{a}^2\right) + \varepsilon_2'\left(\hat{a}^{\dagger 2}\left(\hat{a}^\dagger\hat{a}\right) + \left(\hat{a}^\dagger\hat{a}\right)\hat{a}^2\right), \tag{9}$$

and at fourth order as

$$\begin{aligned}\hat{H}^{(4)} = &-\Delta^{(4)}\left(\hat{a}^\dagger\hat{a}\right) - K^{(4)}\left(\hat{a}^\dagger\hat{a}\right)\left(\hat{a}^\dagger\hat{a}-1\right)\\ &- \lambda^{(4)}\left(\left(\hat{a}^\dagger\hat{a}\right)^3 - 3\left(\hat{a}^\dagger\hat{a}\right)^2 - 2\left(\hat{a}^\dagger\hat{a}\right)\right) + \varepsilon_4^{(4)}\left(\hat{a}^{\dagger 4}+\hat{a}^4\right).\end{aligned} \tag{10}$$

The last term in (10) can also be rewritten as

$$\hat{a}^{\dagger 4}+\hat{a}^4 = \left(\hat{a}^{\dagger 2}+\hat{a}^2\right)^2 - 2\left(\hat{a}^\dagger\hat{a}\right)\left(\hat{a}^\dagger\hat{a}+1\right) - 2. \tag{11}$$

Since again the Hamiltonian contributions $\hat{H}^{(3)}$ and $\hat{H}^{(4)}$ are written in terms of elements of $sp(2,\mathbb{R})$,

$$\hat{H}^{(3)} = -\Delta^{(3)}\hat{F}_z - K^{(3)}\hat{F}_z\left(\hat{F}_z-1\right) + \varepsilon_2^{(3)}\left(\hat{F}_+ + \hat{F}_-\right) + \varepsilon_2'\left(\hat{F}_+\hat{F}_z + \hat{F}_z\hat{F}_-\right), \tag{12}$$

$$\hat{H}^{(4)} = -\Delta^{(4)}\hat{F}_z - K^{(4)}\hat{F}_z\left(\hat{F}_z-1\right) - \lambda^{(4)}\left(\hat{F}_z^3 - 3\hat{F}_z^2 - 2\hat{F}_z\right) + \varepsilon_4^{(4)}\left(\hat{F}_+^2 + \hat{F}_-^2\right), \tag{13}$$

this algebra is the spectrum generating algebra of the Kerr oscillator at order four, that is the Hamiltonian $\hat{H} = \sum_{1\leqslant n\leqslant 4}\hat{H}^{(n)}$, where n denotes the order in the perturbation parameter [9, 33], is a polynomial in the elements $\hat{a}^\dagger\hat{a}, \hat{a}^\dagger\hat{a}^\dagger, \hat{a}\hat{a}$ of the $sp(2,\mathbb{R})$ Lie algebra.

3. Alternative algebraic structure

An alternative spectrum generating algebra is obtained by introducing an auxiliary boson s [44] and constructing the algebra of $u(2)$ as

$$\hat{F}'_- = \hat{s}^\dagger\hat{a}\ ,\ \ \hat{F}'_+ = \hat{a}^\dagger\hat{s}\ ,\ \ \hat{F}'_z = \frac{1}{2}\left(\hat{s}^\dagger\hat{s} - \hat{a}^\dagger\hat{a}\right)\ ,\ \ \hat{N} = \hat{s}^\dagger\hat{s} + \hat{a}^\dagger\hat{a}. \tag{14}$$

The three operators $\hat{F}'_+, \hat{F}'_-, \hat{F}'_z$ satisfy the commutation relations of the Lie algebra $su(2)$,

$$\left[\hat{F}'_z, \hat{F}'_\pm\right] = \pm\hat{F}'_\pm\ ,\ \ \left[\hat{F}'_+, \hat{F}'_-\right] = 2\hat{F}'_z. \tag{15}$$

Together with $\hat{N}$, they are the elements of the Lie algebra of $u(2)$.

We introduce now the operators $\hat{F}'_- = \hat{s}^\dagger\hat{a}$, $\hat{F}'_+ = \hat{a}^\dagger\hat{s}$, $\hat{n} = \hat{a}^\dagger\hat{a}$, $\hat{n}_s = \hat{s}^\dagger\hat{s}$, replace the operators $\hat{s}$ and $\hat{s}^\dagger$ by $\sqrt{\hat{N}}$, and consider the operators

$$\frac{\hat{F}'_-}{\sqrt{\hat{N}}} = \hat{a}\ ,\ \ \frac{\hat{F}'_+}{\sqrt{\hat{N}}} = \hat{a}^\dagger\ ,\ \ \hat{n} = \hat{a}^\dagger\hat{a}\ ,\ \ \frac{\hat{n}_s}{\hat{N}} = \hat{I}. \tag{16}$$

The operators $\hat{a}$, $\hat{a}^\dagger$, $\hat{a}^\dagger\hat{a}$, and the identity operator, $\hat{I}$, form an algebra called the Heisenberg algebra, $h(2)$, with commutation relations

$$\begin{aligned} &\left[\hat{a},\hat{a}^\dagger\right]=\hat{I}, \quad \left[\hat{a}^\dagger,\hat{I}\right]=\left[\hat{a},\hat{I}\right]=0, \\ &\left[\hat{a},\hat{a}^\dagger\hat{a}\right]=\hat{a}\ , \quad \left[\hat{a}^\dagger,\hat{a}^\dagger\hat{a}\right]=-\hat{a}^\dagger. \end{aligned} \tag{17}$$

The algebra $h(2)$ is called the contracted algebra of $u(2)$ [44],

$$u(2)\rightarrow_c h(2)\,. \tag{18}$$

The algebra $h(2)$ is an alternative spectrum generating algebra of the squeeze-driven Kerr oscillator. Calculations for the eigenvalues and eigenvectors of the squeeze-driven Kerr oscillator can therefore also be done making use of the algebra $u(2)$ in the limit $N\rightarrow\infty$. The Hamiltonian $\hat{H}$ at orders 1 and 2 can be rewritten in the $u(2)$ basis as

$$\hat{H}=-\Delta\hat{n}+K\hat{n}\left(\hat{n}-1\right)-\varepsilon_2\left(\hat{a}^\dagger\hat{a}^\dagger\hat{s}\hat{s}+\hat{s}^\dagger\hat{s}^\dagger\hat{a}\hat{a}\right), \tag{19}$$

with contracted form

$$\hat{H}=-\Delta\hat{n}+K\hat{n}\left(\hat{n}-1\right)-\varepsilon_2'\left(\hat{a}^\dagger\hat{a}^\dagger+\hat{a}\hat{a}\right), \tag{20}$$

where $\varepsilon_2'=\varepsilon_2 N$. Hamiltonians as in (19) were considered years ago [51] and are used in the algebraic approach to stretching vibrations of molecules [43].

4. Symmetry and classification of states

The Hamiltonian (1) has a remarkable set of symmetries. For purposes of studying these symmetries, it is convenient to divide by a scale K and consider the dimensionless Hamiltonian

$$\frac{\hat{H}}{K}=-\eta\hat{n}+\hat{n}\left(\hat{n}-1\right)-\xi\hat{P}_2=-\eta'\hat{n}+\hat{n}^2-\xi\hat{P}_2, \tag{21}$$

where $\eta=\Delta/K$ and $\xi=\varepsilon_2/K$ are control parameters and $\eta'=\eta+1$. In what follows, we analyze first the symmetries of parts of the Hamiltonian (21), namely $-\eta\hat{n}+\hat{n}(\hat{n}-1)$ in section 4.1 and $\hat{n}(\hat{n}-1)-\xi\hat{P}_2$ in section 4.2, before investigating the complete Hamiltonian in section 4.3.

4.1. Symmetries of the Hamiltonian $-\eta\hat{n}+\hat{n}(\hat{n}-1)$

We consider first the Hamiltonian

$$\hat{H}_1=\frac{\hat{H}}{K}=-\left(\eta+1\right)\hat{n}+\hat{n}^2=-\eta'\hat{n}+\hat{n}^2. \tag{22}$$

The spectrum of eigenvalues of this Hamiltonian, counted from the lowest state, is shown in figure 1. It is divided into two parts (phases) with separatrix $E_s=\eta/2+\eta^2/4$ marked in the figure with a dashed black line.

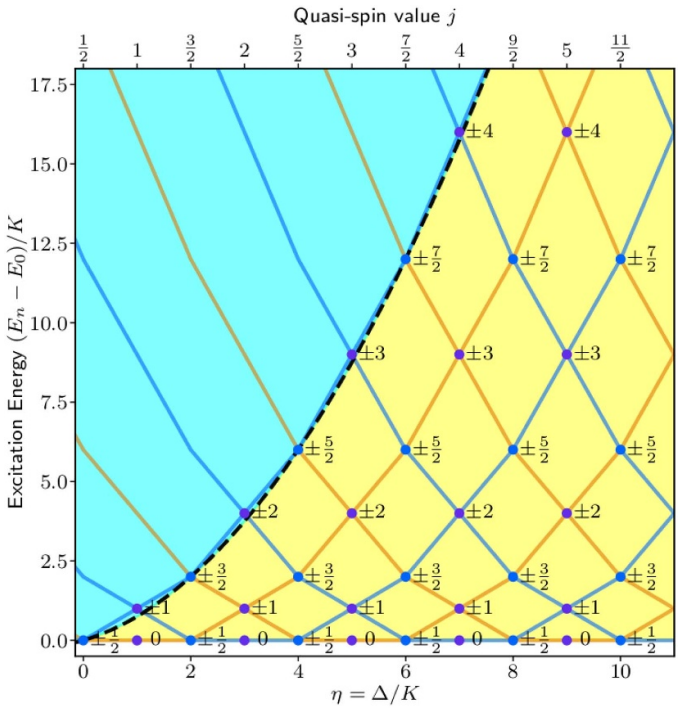

Figure 1. Excitation energy of the Hamiltonian (22) as a function of the control parameter $\eta = \Delta/K$ (ratio of detuning to Kerr coefficient). The quasi-spin $|j,m\rangle$ classification of the degenerate states with energies $E(\eta = \text{odd}) = m^2$, $E(\eta = \text{even}) = m^2 - \frac{1}{4}$ is included. Crossings are marked with blue dots and labelled by their associated m values. The separatrix, marked with a dashed black line, is $E_s = \eta/2 + \eta^2/4$. The parity of the eigenstates is positive (orange) and negative (blue). The two phases are marked by blue and yellow backgrounds.

To the left of the separatrix (blue filled region), states are singly degenerate with $u(1)$ symmetry, $u(1) \doteq \hat{a}^\dagger \hat{a}$, and eigenvalues

$$E = -(\eta + 1)n + n^2 = -\eta' n + n^2. \tag{23}$$

To the right of the separatrix (yellow filled region) and for $\eta' = \eta + 1 = \text{integer}$, degeneracies occur. These degeneracies are due to a remarkable (and hitherto unknown) quasi-spin symmetry $su(2)$.

The degeneracy points can be characterized by quasi-spin quantum numbers $|j,m\rangle$. The values of the quasi-spin are $j = \frac{\eta'}{2} = \frac{\eta+1}{2}$, as given in table 1. For each j value, the values of m are

$$\begin{aligned} &m = \pm j, \pm(j-1), \ldots, \pm 1/2\ ;\ \ j = \text{half-integer}\ ;\ \ \eta = \text{even}, \\ &m = \pm j, \pm(j-1), \ldots, 0\ ;\ \ j = \text{integer}\ ;\ \ \eta = \text{odd}. \end{aligned} \tag{24}$$

The eigenvalues E of $\hat{H}/K$, counted from the lowest state, are

$$E = m^2 - \frac{1}{4}\ ;\ \ m = \pm\frac{1}{2}, \pm\frac{3}{2}, \pm\frac{5}{2}, \ldots, \pm j, \tag{25}$$

Table 1. The values of the quasi-spin are $j = \frac{\eta'}{2} = \frac{\eta+1}{2}$.

η'	1	2	3	4	5	...
η	0	1	2	3	4	...
j	1/2	1	3/2	2	5/2	...

for half integer j (even η) and

$$E = m^2 \; ; \;\; m = 0, \pm 1, \pm 2, \ldots, \pm j, \tag{26}$$

for integer j (odd η). Both sets of eigenvalues correspond to the dynamic symmetry $su(2) \supset so(2)$. Note that each eigenvalue is doubly degenerate, $\pm m$, except for $m = 0$, when it is singly degenerate. This result can be verified from figure 1 where the values of j and m at the degeneracy points are shown.

To elucidate this quasi-spin symmetry, it is convenient to construct the representations $|j,m\rangle$ with two boson operators $\hat{b}_1, \hat{b}_2$ (see [44]) with eigenvalues of the number operators $\hat{n}_1, \hat{n}_2$ satisfying $n_1 + n_2 = N$. The values of j and m are

$$j = \left(\frac{n_2 + n_1}{2}\right), \quad m = \left(\frac{n_2 - n_1}{2}\right). \tag{27}$$

For example, the values of m for the representation $n_2 + n_1 = N = 5$, $j = 5/2$, $\eta' = 5$, $\eta =$ even $= 4$ are given in table 2. One can verify from figure 1 that the doubly degenerate states at $\eta' = 5, \eta =$ even $= 4$ have precisely the values of n_1, n_2 as given in table 2. Similarly, the values of m for the representation $n_2 + n_1 = N = 4$, $\eta' = 4$, $\eta =$ odd $= 3$ are given in table 3 and are precisely those in figure 1, with a singly degenerate state at zero energy and doubly degenerate states with energy given by m^2. The degeneracies stem from the fact that for a given N, there are two values of n_1 and n_2 satisfying $N = n_1 + n_2$, except for $N =$ even, $n_1 = n_2 = N/2$, where the two values merge into a single value. The dynamic symmetry stems from the simple identity

$$m^2 = \left(\frac{n_2 - n_1}{2}\right)^2 = \frac{N^2}{4} + \left(n_1^2 - N n_1\right), \tag{28}$$

which, for $\eta' = N$, gives energies counted from the lowest state

$$E = n_1^2 - \eta' n_1. \tag{29}$$

In terms of two boson operators $\hat{b}_1$ and $\hat{b}_2$, the wave functions of the degenerate states can be written as

$$|n_1, n_2\rangle = \frac{1}{\sqrt{n_1!\,(N - n_1)!}} \left(\hat{b}_2^\dagger\right)^{N - n_1} \left(\hat{b}_1^\dagger\right)^{n_1} |0\rangle. \tag{30}$$

The notation $|n_1, n_2\rangle$ can be converted to the usual quasi-spin notation by means of (27) giving

$$|j,m\rangle = \frac{1}{\sqrt{(j-m)!\,(j+m)!}} \left(\hat{b}_2^\dagger\right)^{j+m} \left(\hat{b}_1^\dagger\right)^{j-m} |0\rangle. \tag{31}$$

Note that the degenerate states are related by the transformation $m \to -m$ (also related in quantum mechanics to time reversal T). In the two boson construction, it is also possible to

Table 2. Values of m for the representation $n_2+n_1=N=5$, $j=5/2$, $\eta'=5$, $\eta=\text{even}=4$.

n_1	n_2	m	m^2	$m^2-1/4$
0	5	5/2	25/4	6
1	4	3/2	9/4	2
2	3	1/2	1/4	0
3	2	−1/2	1/4	0
4	1	−3/2	9/4	2
5	0	−5/2	25/4	6

Table 3. Values of m for the representation $n_2+n_1=N=4$, $\eta'=4$, $\eta=\text{odd}=3$.

n_1	n_2	m	m^2
0	4	2	4
1	3	1	1
2	2	0	0
3	1	−1	1
4	0	−2	4

associate a parity $P=(-)^{n_1}$ to the states. For $N=\text{odd}, \eta=\text{even}$, the two degenerate states have opposite parity, while for $N=\text{even}, \eta=\text{odd}$, the degenerate states have the same parity. Thus, for $N=\text{odd}, \eta=\text{even}$, the degenerate states change sign under PT transformation, while for $N=\text{even}, \eta=\text{odd}$ they do not. All properties of the degenerate points for integer values of η can be verified in figure 1.

4.2. *Symmetries of the Hamiltonian* $\hat{n}(\hat{n}-1)-\xi\hat{P}_2$

The Hamiltonian

$$\hat{H}_2=\frac{\hat{H}}{K}=\hat{n}\,(\hat{n}-1)-\xi\hat{P}_2 \tag{32}$$

is of importance in the theory of quantum phase transitions (QPTs) and of their associated ESQPTs [47–49]. Its structure in terms of elements of the $sp(2,\mathbb{R})\sim su(1,1)$ algebra is

$$\frac{\hat{H}}{K}=\hat{F}_z\left(\hat{F}_z-1\right)-2\xi\hat{F}_x, \tag{33}$$

and is therefore in the same universality class of the one-dimensional vibron model [43, 51], $\hat{H}_{\text{vibron}}=\varepsilon\hat{F}_z+\delta\hat{F}_z^2-A\hat{F}_x^2$ and of the Lipkin-Meshkov-Glick model [52], $\hat{H}_{\text{LMG}}=\omega\hat{F}_z+v\left(F_x^2-F_y^2\right)$. Its spectrum generating algebra is $sp(2,\mathbb{R})$ with two subalgebras

$$sp\,(2,\mathbb{R})\begin{cases}\nearrow\ u\,(1)\\ \searrow\ so\,(1,1)\end{cases}, \tag{34}$$

where $u(1) \doteqdot \hat{a}^\dagger \hat{a} = \hat{F}_z$ and $so(1,1) \doteqdot \frac{1}{2}\left(\hat{a}^\dagger \hat{a}^\dagger + \hat{a}\hat{a}\right) = \hat{F}_x$. Since $sp(2,\mathbb{R})$ is non-compact, in order to study its symmetries, it is convenient to consider the alternative algebraic structure of the Heisenberg algebra $u(2) \to_c h(2)$. The algebra of $u(2) \supset su(2)$ has two subalgebras

$$u(2) \supset su(2) \begin{array}{c} \nearrow \quad u(1) \\ \\ \searrow \quad so(2) \end{array} . \tag{35}$$

States are characterized by the quantum numbers

$$\begin{aligned} u(1) &: |[N], n\rangle , \\ so(2) &: |[N], \sigma\rangle , \end{aligned} \tag{36}$$

where n are the eigenvalues of $\hat{a}^\dagger \hat{a}\,(n = 0, 1, \ldots, N)$ and σ those of $\hat{a}^\dagger \hat{s} + \hat{s}^\dagger \hat{a} (\sigma = \pm N, \pm(N-2), \pm(N-4), \ldots, \pm 1$ or 0, for $N =$ odd or even). The $\pm$ sign comes from the fact that $so(2)$ is an orthogonal algebra in even dimension [44]. The notation $|[N], \sigma\rangle$ can be converted to the usual $|j, m\rangle$ notation of the quasi-spin algebra $su(2)$ by

$$\left| j = \frac{N}{2}, m = \frac{\sigma}{2} \right\rangle , \quad m = \pm\frac{N}{2}, \pm\left(\frac{N}{2} - 1\right), \ldots, \pm\frac{1}{2} \text{or } 0, \tag{37}$$

for N odd or even. The dimension of the representation is

$$\dim [N] = 2j + 1 = N + 1. \tag{38}$$

The value of j is half-integer (integer) for N odd (even). Another notation, used in molecular physics, is [43, 51]

$$\left| [N], v^{\pi'} = \frac{N - \sigma}{2} \right\rangle , \quad \pi' = \pm , \quad v = 0, 1, \ldots, \frac{N-1}{2} \text{or } \frac{N}{2}, \tag{39}$$

for N odd or even. The quantum number v is called the vibrational quantum number and π' is the sign of σ (or of m). In the large system size limit, $N \to \infty$, the contracted $so(2)$ operator becomes

$$\left(\hat{a}^\dagger \hat{s} + \hat{s}^\dagger \hat{a}\right) \to_c \frac{\left(\hat{F}_+ + \hat{F}_-\right)}{\sqrt{N}} = \left(\hat{a}^\dagger + \hat{a}\right). \tag{40}$$

Another important operator is the quadratic Casimir operator of $so(2)$

$$\hat{C}_2 = \left(\hat{a}^\dagger \hat{s} + \hat{s}^\dagger \hat{a}\right)^2 = \hat{a}^\dagger \hat{a}^\dagger \hat{s}\hat{s} + \hat{s}^\dagger \hat{s}^\dagger \hat{a}\hat{a} + 2\hat{a}^\dagger \hat{a}\hat{s}^\dagger \hat{s} + \hat{a}^\dagger \hat{a} + \hat{s}^\dagger \hat{s}, \tag{41}$$

with eigenvalues

$$\left\langle \hat{C}_2 \right\rangle = \sigma^2 = 4m^2. \tag{42}$$

With the vibrational quantum number v, the eigenvalues of $\hat{C}_2$ can be written as

$$\left\langle \hat{C}_2 \right\rangle = N^2 - 4Nv\left(1 - \frac{v}{N}\right), \quad v = 0, 1, \ldots, \frac{N-1}{2} \text{or } \frac{N}{2}, \tag{43}$$

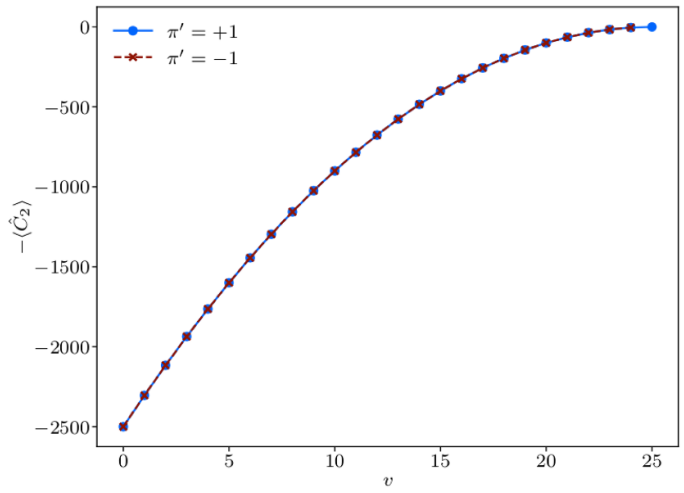

Figure 2. Eigenvalues of the operator $-\hat{C}_2$ as a function of v for $N = 50$. Each point is doubly degenerate, $\pi' = \pm$, except $v = N/2 = 25$.

for N odd or even and $\pi' = \pm$. The eigenvalues of $\hat{C}_2$ are doubly degenerate $\pi' = \pm$, except for $\sigma = 0$ ($v = N/2$, even N) which is singly degenerate. Introducing the pairing operator of $su(2)$

$$\hat{P}_2' = \hat{a}^\dagger\hat{a}^\dagger\hat{a}\hat{a} + \hat{s}^\dagger\hat{s}^\dagger\hat{s}\hat{s} - \hat{a}^\dagger\hat{a}^\dagger\hat{s}\hat{s} - \hat{s}^\dagger\hat{s}^\dagger\hat{a}\hat{a} = N^2 - \hat{C}_2, \tag{44}$$

one has

$$\left\langle \hat{P}_2' \right\rangle = N^2 - \sigma^2 = 4Nv\left(1 - \frac{v}{N}\right), \quad v = 0, 1, \ldots, \frac{N-1}{2} \text{or } \frac{N}{2}, \tag{45}$$

for N odd or even and $\pi' = \pm$. The eigenvalues of $-\hat{C}_2$ are shown in figure 2.

The contracted form of the operator $\hat{C}_2$ is

$$\hat{C}_2 \rightarrow_c N\left(\hat{a}^\dagger\hat{a}^\dagger + \hat{a}\hat{a}\right) + 2\hat{n}\left(N - \hat{n}\right) + N, \tag{46}$$

where $\hat{n}_s = \hat{s}^\dagger\hat{s}$ has been replaced by $N - \hat{n}$. Unfortunately, because of the additional terms, the eigenvalues of the pairing operator of $sp(2,\mathbb{R})$, $\hat{P}_2 = \hat{a}^\dagger\hat{a}^\dagger + \hat{a}\hat{a}$, cannot be obtained simply from those of the quadratic Casimir operator of $so(2)$ and must be calculated numerically.

Going from $su(2)$ to $sp(2,\mathbb{R})$, while the $u(1)$ classification $|[N], n\rangle$ remains the same, the classification $|[N], \sigma\rangle$ in terms of a quasi-spin j and component m needs to be modified, since there is a doubling of representations [53]. To this end, we consider the eigenvalues of the operator

$$-\hat{P}_2 = -\left(\hat{a}^{\dagger 2} + \hat{a}^2\right) = -2\hat{F}_x. \tag{47}$$

Introducing the parity $\pi = (-)^n$, for a given N, there are two representations, one with even parity $\pi = +$ and one with odd parity $\pi = -$, with values of j given by

$$\begin{array}{lllll} N = 4\nu & ; & j = \frac{N}{4},\ \pi = + & ; & j = \frac{N}{4} - \frac{1}{2},\ \pi = - \\ N = 4\nu + 2 & ; & j = \frac{N}{4},\ \pi = + & ; & j = \frac{N}{4} - \frac{1}{2},\ \pi = - \\ N = 4\nu + 1 & ; & j = \frac{N-1}{4},\ \pi = + & ; & j = \frac{N-1}{4},\ \pi = - \\ N = 4\nu + 3 & ; & j = \frac{N-1}{4},\ \pi = + & ; & j = \frac{N-1}{4},\ \pi = - \end{array} \tag{48}$$

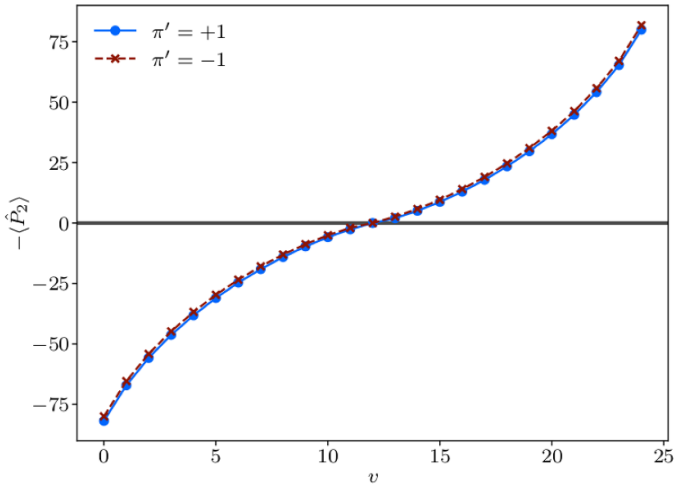

Figure 3. Eigenvalues of the operator $-\hat{P}_2$ as a function of v for $N = 50$.

and $\nu = 1, 2, 3, \ldots$. The values of m are

$$m = j, j-1, \ldots, -(j-1), -j = j - v, \tag{49}$$

with v given by

$$\begin{array}{lllll} N = \text{even} & ; & v = 0, 1, \ldots, \frac{N}{2}\ , & \pi = + & ; \quad v = 0, 1, \ldots, \left(\frac{N}{2} - 1\right)\ , \quad \pi = -, \\ N = \text{odd} & ; & v = 0, 1, \ldots, \frac{N-1}{2}\ , & \pi = + & ; \quad v = 0, 1, \ldots, \frac{N-1}{2}\ , \quad \pi = -. \end{array} \tag{50}$$

For example, for $N = 50$, the even parity states are classified by the representation $j = \frac{25}{2}, -\frac{25}{2} \leqslant m \leqslant +\frac{25}{2}$, with a total number of states $2j + 1 = 26$. The odd parity states are classified by the representation $j = \frac{24}{2} = 12, -12 \leqslant m \leqslant +12$, with a total number of states $2j + 1 = 25$. For each representation, the eigenvalues come in pairs, corresponding to positive and negative values of $m = \pm j, \pm(j-1), \ldots, \pm 1/2$ or 0 for j half-integer or integer (π', $m \to -m$), except for $m = 0$. The results of a numerical diagonalization are shown in figure 3 for $N = 50$. For each parity $\pi = \pm$, there are two branches with $\pi' = \pm$. Note that $\pi \neq \pi'$.

In the limit $N \to \infty$, the spectrum of the operator $-\hat{P}_2$ is a straight line extending from $-N$ to $+N$. The line is doubled, one for each parity $\pi = \pm$. This property stems from the fact that the operator $\hat{F}_x$ changes n by ± 2 units and thus conserves parity. The spectrum of energies can be written as

$$E = -2m. \tag{51}$$

The spectrum extends to $\pm\infty$ due to the non-compact nature of $sp(2, \mathbb{R})$, the representations of which are discrete but infinite dimensional, $-\infty < m < +\infty$. Note that in the $N \to \infty$ limit, the two representations, j_{even} and j_{odd}, which form the two components of the $sp(2, \mathbb{R})$ representation, become degenerate. However, as seen from figure 3, the convergence to the asymptotic limit is very slow, and it is far from reached at $N = 50$.

Consider now the Hamiltonian (32). The spectrum of this Hamiltonian, calculated numerically in the $u(1)$ basis with $n_{\max} \equiv N = 800$, is shown in figure 4. The value of $N = 800$ is

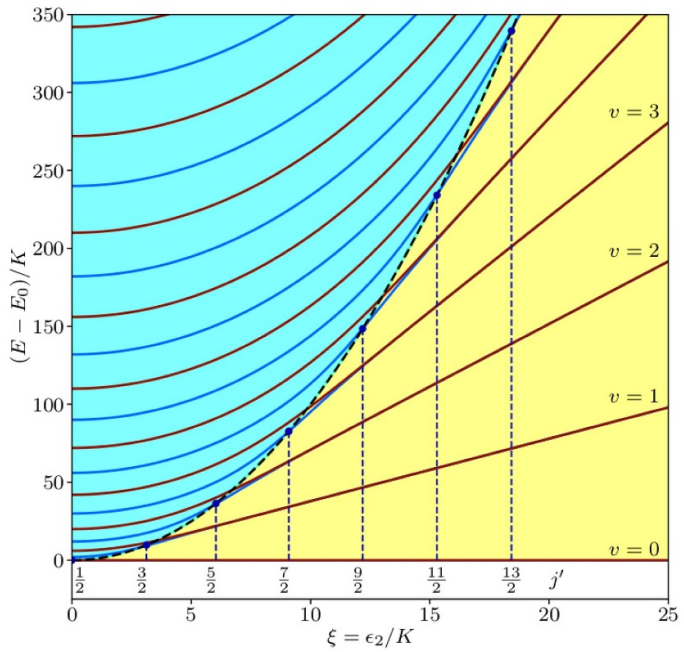

Figure 4. Excitation energy of Hamiltonian (32) as a function of the control parameter ξ. Quasi-spin $|j',m'\rangle$ classification of the degenerate states at the point of maximal rate of approach, $\xi_c=\pi v$ is shown. The separatrix, marked with a dashed black line, is $E_s=\xi^2$. The size of the Fock space is truncated at $N=800$. States to the left of the separatrix are singly-degenerate with positive (blue) and negative (red) parity. States to the right of the separatrix are labeled by the number $v=0,1,2,\ldots$ of equation (39) and are doubly degenerate with parity $\pm$.

chosen here in order that the eigenvalues in the range $0\leqslant\xi\leqslant 25$ of the figure are well converged. While the convergence of the eigenvalues of the pairing term $\hat{P}_2$ is very slow due to its non-compacteness, the convergence of the Hamiltonian (32) is faster due to the presence of the Kerr term $\hat{n}(\hat{n}-1)$ which increases as n^2 for large n. The spectrum exhibits an ESQPT [37] similar to that encountered in the one-dimensional vibron model and the Lipkin-Meshkov-Glick model [49, 54, 55]. It is divided into two parts (phases) with separatrix E_s. To the left of the separatrix, states are singly degenerate with $u(1)$ symmetry. To the right, states are doubly degenerate with $so(2)$ symmetry. The degenerate states have opposite parity π. The classification of states in terms of a quasi-spin $|j',m'\rangle$ is, however, as discussed in the paragraphs above, rather complicated. At values of $\xi=4v=0,4,8,12,\ldots$ states can be classified by a quasi-spin $|j',m'\rangle$ with $j'=\xi/4+1/2=1/2,3/2,5/2,\ldots$ and $-j'\leqslant m'\leqslant+j'$, where we have used j',m' instead of j,m to emphasize that the quasi-spin here is not the same of the previous subsection. This classification is also valid at values of $\xi_c=(\pi/4)4v$, which are the values of the critical points as obtained from the maximal rate of approach [9] and shown with circles in figure 4.

In the large N limit, the separatrix is $E_s=\xi^2$, the energy of the states to the right of the separatrix is $E_v=4\xi v\,(v=0,1,2,3\ldots)$ and the critical value obtained by the condition $E_s=E_v$ is $\xi_c=4v$. The values of E_v to which the numerical calculation converges cannot be obtained in explicit analytic form. By analogy with (45), which applies to the compact version of the

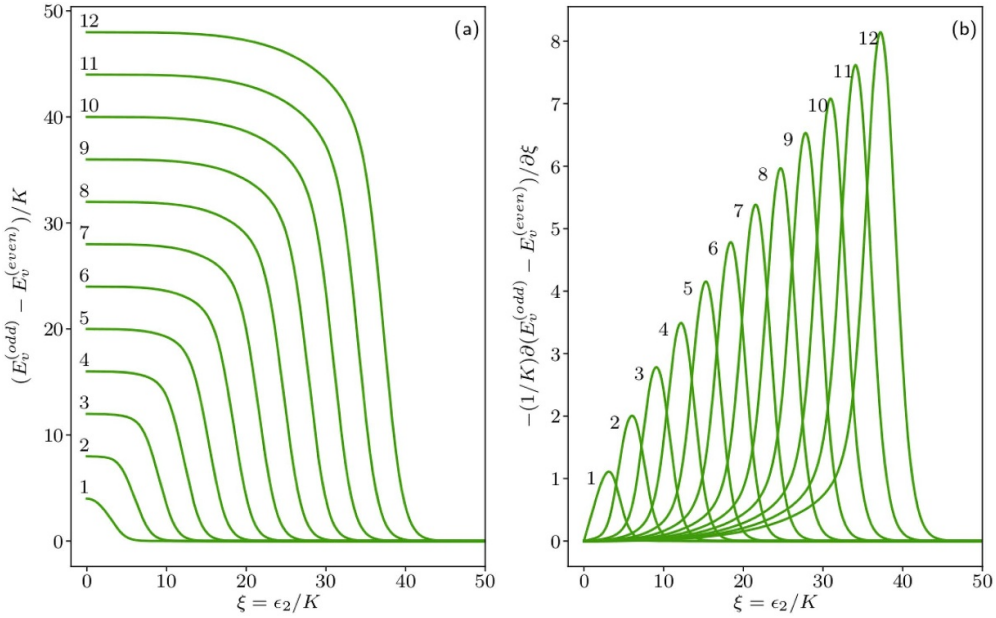

Figure 5. Panel (a): The gap $(E_v^{(\mathrm{odd})} - E_v^{(\mathrm{even})})/K$ as a function of ξ for $v = 1, \ldots, 12$. Panel (b): The derivative of the gap $-\frac{1}{K}\partial(E_v^{(odd)} - E_v^{(even)})/\partial\xi$ as a function of ξ for $v = 1, \ldots, 12$. The critical value ξ_c is the value of ξ at the maximum of the derivative [9]. The gaps go to zero as the separatrix is crossed for each v as a function of ξ. To the right of the separatrix, states are doubly degenerate with $E_v^{(odd)} = E_v^{(even)}$ (parity $\pm$).

operator, $\hat{P}_2'$, we suggest an approximate expression for the energy of the states to the right of the separatrix to be

$$E_v = 4\xi v\left(1 - \frac{v}{N_{\mathrm{eff}}}\right) \ , \quad v = 0, 1, 2, 3, \ldots \tag{52}$$

where $N_{\mathrm{eff}} = N/2$ and N is the value $n_{\max}$ of states kept in the numerical calculation. The determination of the critical value ξ_c depends on its definition. In [9], the critical value is defined as the point of maximal rate of approach determined by the inflection point in the energy gaps, as illustrated in figure 5. The value so determined is $\xi_c = 0.775(4v) \cong \pi v$ [9]. However, at this point, the gap is still large. Another possible determination is by a linear extrapolation of the gaps $(E_{\mathrm{odd}} - E_{\mathrm{even}})$. This determination is closer to the expected values of the ESQPT. Finally, another determination is the location at which the energy difference $(E_{\mathrm{odd}} - E_{\mathrm{even}})$ is less than a given fraction of the energy semi-sum $(E_{\mathrm{odd}} - E_{\mathrm{even}})/2$. We use here $(E_{\mathrm{odd}} - E_{even}) \leqslant 0.005(E_{\mathrm{odd}} + E_{\mathrm{even}})/2$. The values determined by these three methods are shown in figure 6(a).

All three results produce similar results. Particularly interesting is the result of the maximal rate of approach, which is a straight line with slope π, as expected in a semi-classical approximation to the Hamiltonian $\hat{H}$ [9]. However, this result is not accurate for small v, since at this point the gap is still large. For small v, the critical value that best describes the merging of the two energies $E_{\mathrm{odd}} - E_{\mathrm{even}}$ (the so-called kissing point [9]) is the linear extrapolation. The values of E_c at the critical point ξ_c determine then the separatrix E_s. The values so determined

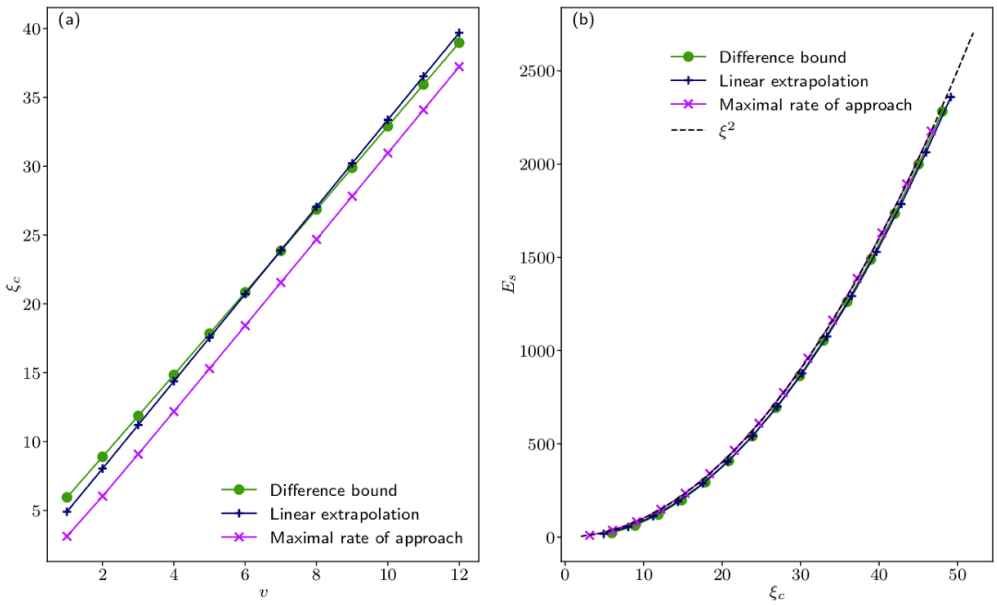

Figure 6. Panel (a): The values of the critical point ξ_c as a function of v as obtained by the three methods: maximal rate of approach (cross) [1], linear extrapolation (plus), and difference bound (circle). Panel (b): The values of the separatrix E_s as a function of ξ as obtained by the three methods of panel (a). The semiclassical result [37] is shown with a dashed line.

are shown in figure 6(b). Again here all three methods produce similar results all of which are very close to the semi-classical expression $E_s = \xi^2$ [37].

4.3. Symmetries of the Hamiltonian $-\eta\hat{n} + \hat{n}(\hat{n}-1) - \xi\hat{P}_2$

The spectrum of the Hamiltonian (21), $\hat{H}/K = -\eta\hat{n} + \hat{n}(\hat{n}-1) - \xi\hat{P}_2$, as a function of η for a fixed value of $\xi = 1$ is shown in figure 7(a). The spectrum is now separated into three phases.

Phase 1 is separated from phase 2 by a separatrix approximately given by

$$E_s = \frac{\eta}{2} + \frac{\eta^2}{4} + \eta\xi. \tag{53}$$

To the left of the separatrix, given by (53), states are still singly degenerate with $u(1)$ symmetry. To the right of this separatrix, states split into phases 2 and 3, with another separatrix, the energy of which, E_s', is approximately given by

$$E_s' = \eta\xi. \tag{54}$$

In the intermediate phase 2, to the left of the new separatrix (54), states resemble those of phase 2 of the Hamiltonian $\hat{H}_1 = -\eta\hat{n} + \hat{n}(\hat{n}-1)$ in figure 1, with braiding which decreases as η increases. However, while at even values of $\eta = 2,4,6,\ldots$ states maintain the double degeneracy of the $so(2)$ symmetry of figure 1, at odd values of $\eta = 1,3,5,\ldots$ the degeneracy is lifted and replaced by a new $so(2)$ symmetry, as will be discussed in the next section. To be precise, each half-integer j quasi-spin representation that occurs at even values, $\eta = 2,4,6,\ldots$,

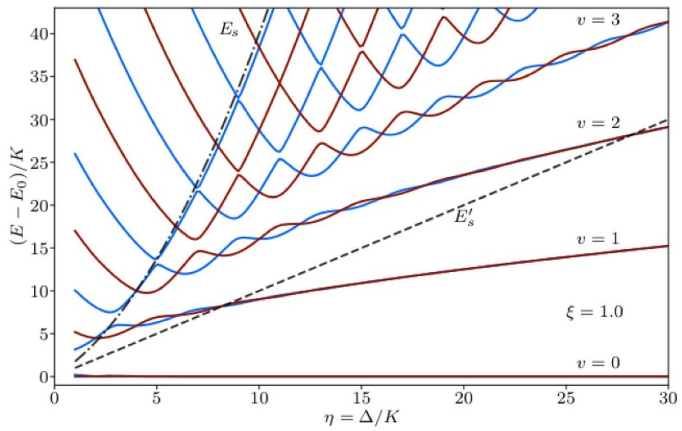

Figure 7. Spectrum of the Hamiltonian (21) as a function of η for $\xi = 1$. The approximate separatrices $E_s = \eta/2 + \eta^2/4 + \eta\xi$ and $E'_s = \eta\xi$ are shown as black dash-dotted and dashed lines, respectively. To the left of the separatrix E_s, Phase I, states are singly degenerate with positive (red) and negative (blue) parity. In between the separatrices E_s and E'_s, Phase II, braiding occurs. To the right of the separatrix, Phase III, states are doubly degenerate with parity $\pm$. They are labeled by the quantum number $v = 0, 1, 2, \ldots$ of equation (39). The calculations have been carried out with a Fock basis with $N = 800$.

is simply moved up. The crossings are allowed since the degenerate states, composed by one positive and one negative parity state ($\pi = \pm$) have different symmetries. Each integer j quasi-spin representation, which occurs for odd values $\eta = 1, 3, 5, \ldots$, is instead modified. In this case states have the same parity, the crossing is forbidden and the degeneracy is lifted. The different character of the crossings at even and odd values of the η control parameter have a strong impact on the system dynamics and, in particular, on the possibility of tunneling between different regions of the system's phase space [36]. Similar effects have been recently uncovered in the Lipkin-Meshkov-Glick model ESQPT [56].

In phase 3, which lies to the right of the new separatrix (54), states resemble those of phase 2 of Hamiltonian $\hat{H}_2 = \hat{n}(\hat{n} - 1) - \xi\hat{P}_2$ in figure 4. States can be classified by a vibrational quantum number $v = 0, 1, 2, \ldots$. (or by a quasi-spin $|j', m'\rangle$ with $j' =$ half-integer, $m' = \pm 1/2, \pm 3/2, \ldots$).

As it will be shown in the next section, the location of the degeneracies for even $\eta = 2, 4, 6, \ldots$ in the intermediate phase 2 remains the same even for non-perturbative values of ξ, due to the fact that the quasi-spin quantum numbers retain the same half-integer values, while for odd $\eta = 1, 3, 5, \ldots$, the degeneracies change from those of integer j to those of half-integer j.

5. Other Hamiltonians and the stability of the solutions of the squeeze-driven Kerr Hamiltonian

In view of the fact that additional Hamiltonians can be, in principle, engineered and experimentally studied [9, 34], we consider in this section the effect of adding parametric terms to the Kerr nonlinearity. We begin by investigating

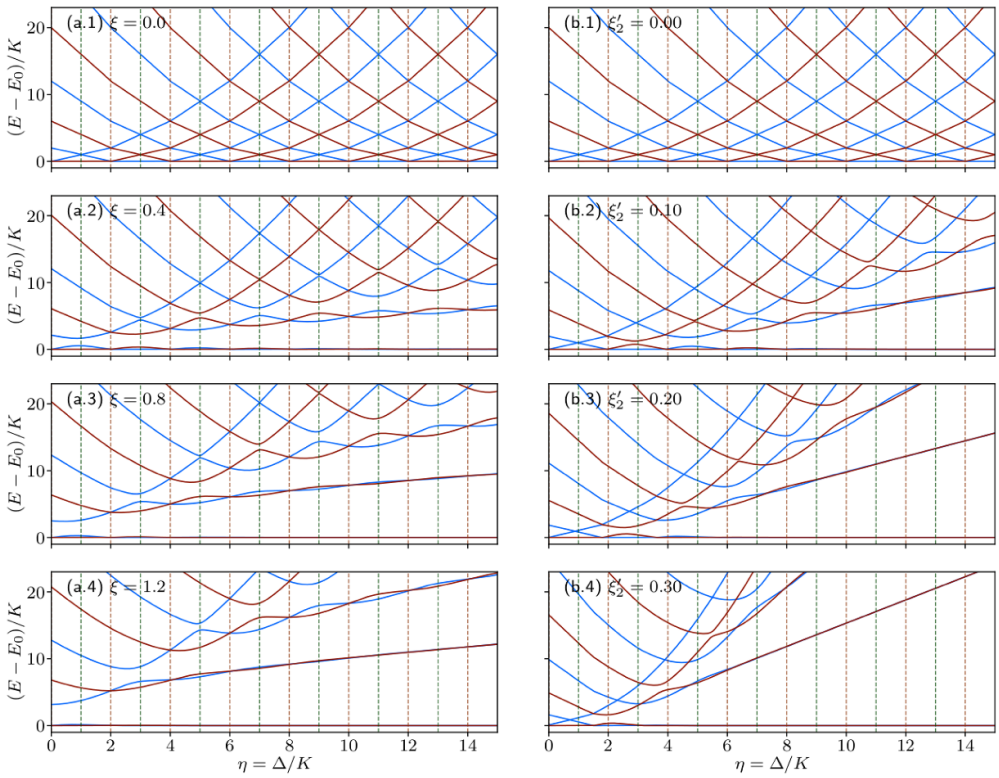

Figure 8. Panels (a.1)–(a.4): Spectrum of the Hamiltonian (56) as a function of η for different values of ξ. Panels (b.1)–(b.4): Spectrum of the Hamiltonian (59) as a function of η for different values of ξ_2'. All panels: The integer values of η are shown by vertical dotted lines. The blue (red) color denotes even (odd) parity states.

$$\frac{\hat{H}}{K} = -\eta\hat{n} + \hat{n}\,(\hat{n}-1) - \xi_i\hat{P}_i, \tag{55}$$

where $\hat{P}_i$ is a generic term and ξ_i its strength.

Consider first the addition of the term $-\xi\hat{P}_2$, which takes the Hamiltonian of the Kerr oscillator (22) to that of the squeeze-driven Kerr oscillator (21), copied here once again,

$$\frac{\hat{H}}{K} = -\eta\hat{n} + \hat{n}\,(\hat{n}-1) - \xi\hat{P}_2. \tag{56}$$

Hamiltonian (22) has, as discussed in section 4.1, a quasi-spin symmetry with states characterized by the quasi-spin quantum numbers $|j,m\rangle$, with integer j at $\eta = 1,3,5\ldots$ and half-integer j at $\eta = 2,4,6,\ldots$. A remarkable property of the squeeze-driven Kerr Hamiltonian (56) is that the quasi-spin representations $|j,m\rangle$ with $j =$ half-integer (even $\eta = 2,4,6,\ldots$) are not altered by the term $-\xi\hat{P}_2$, that is, the degeneracies remain at the same points $\eta = 2,4,6\ldots$ but at larger energy values. This is clearly seen in figures 8(a.1)–(a.4), where the spectrum of the Hamiltonian (56) is shown as a function of η for different values of ξ. This property, first found in [9–11], is of great importance for possible applications of KPO to quantum computing, and is related to the newly discovered quasi-spin symmetry which occurs for integer values of $\eta = \Delta/K$.

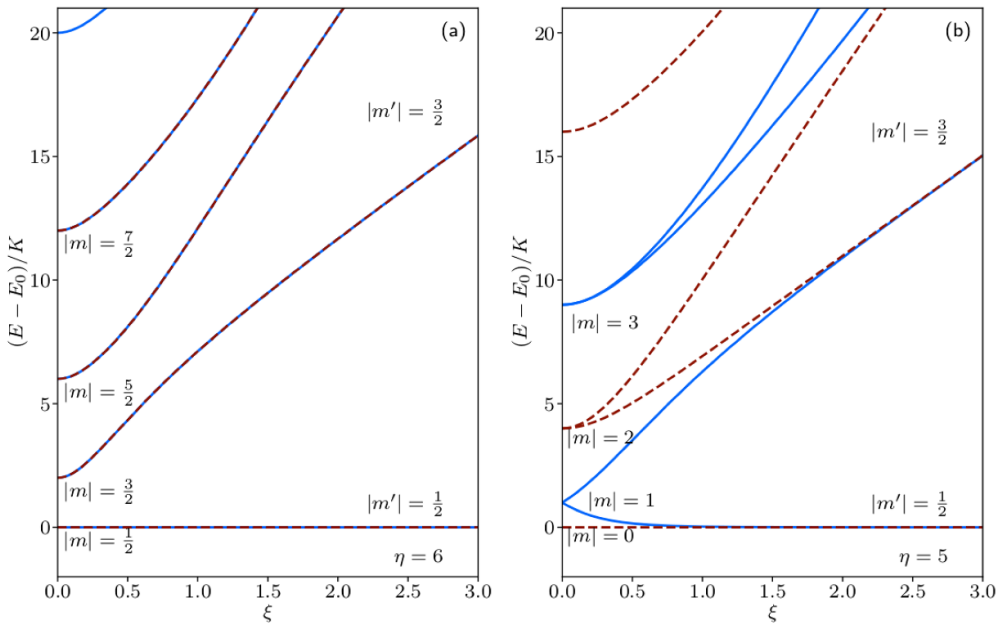

Figure 9. Panel (a): Behavior of the different components of the quasi-spin $j = 7/2, \eta = 6$ as a function of ξ. The degeneracies persist even for non-perturbative values of ξ. Panel (b): Same as (a) but for $j = 3, \eta = 5$. The degeneracies in panel (b) are split. In the asymptotic limit, not yet reached in the figure, the degeneracies become those of $j' = 7/2$. See also [30]. Both panels: solid blue lines are for even parity states and dashed red lines for odd parity states.

The behavior of the different m components of the quasi-spin j as a function of ξ is shown in figure 9(a) for the representation $j = 7/2$ ($\eta = 6$). At $\xi = 0$, the energies are given by (25), $E = m^2 - 1/4$. On the contrary, the quasi-spin representations with integer j (odd $\eta = 1, 3, 5, \ldots$) are affected in such a way that the degeneracies change from those of integer j, with $m = 0, \pm 1, \pm 2, \ldots$, to those of half-integer j, with $m = \pm 1/2, \pm 3/2, \ldots$. The behavior of the different m components of the quasi-spin j as a function of ξ in the odd η case is shown in figure 9(b) for the representation $j = 3$ ($\eta = 5$). At $\xi = 0$, the energies are $E = m^2$, as given in (26). These properties persist even for non-perturbative values of ξ.

Going to third and fourth orders in the boson expansion of the Hamiltonian (see equations (9) and (10)), we observe that some of the additional terms are a renormalization of lower order terms, $\Delta^{(3)}, K^{(3)}, \varepsilon_2^{(3)}, \Delta^{(4)}, K^{(4)}, \lambda^{(4)}$, but two new terms appear, one of order 3,

$$\varepsilon_2' \left(\hat{n} \cdot \hat{P}_2 \right) \equiv \varepsilon_2' \left(\hat{a}^{\dagger 2} \left(\hat{a}^\dagger \hat{a} \right) + \left(\hat{a}^\dagger \hat{a} \right) \hat{a}^2 \right), \tag{57}$$

where the dot indicates normal ordering, and one of order 4,

$$\varepsilon_4^{(4)} \hat{P}_4 \equiv \varepsilon_4^{(4)} \left(\hat{a}^{\dagger 4} + \hat{a}^4 \right). \tag{58}$$

The spectrum of the Hamiltonian

$$\frac{\hat{H}}{K} = -\eta \hat{n} + \hat{n} \left(\hat{n} - 1 \right) - \xi_2' \hat{n} \cdot \hat{P} \tag{59}$$

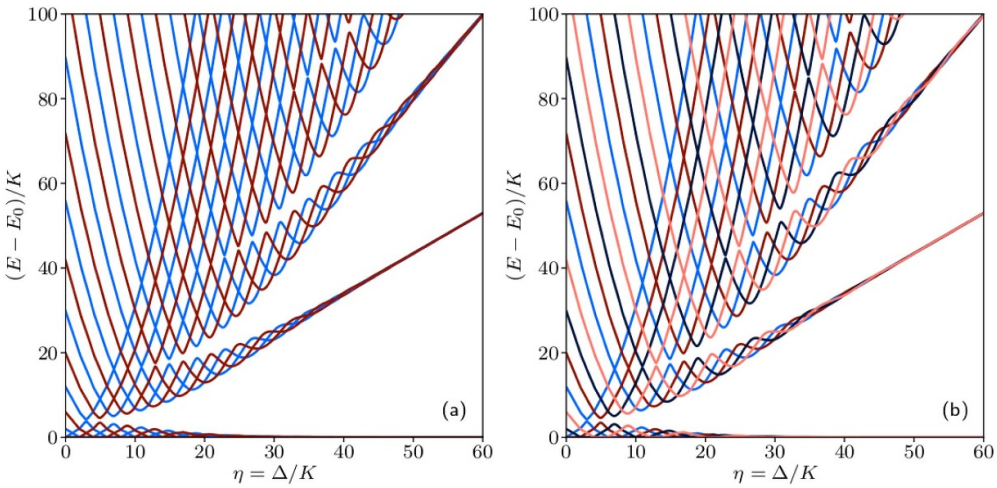

Figure 10. Panel (a): Spectrum of the Hamiltonian (60) for $\xi_4 = 0.05$. The blue color denotes positive parity states and the red color negative parity states with $\mathrm{mod}\,2 \oplus \mathrm{mod}\,2$ coloring. Panel (b): Spectrum of the same Hamiltonian as a function of η with $\mathrm{mod}\,4$ coloring, with red tones for odd parity and blue tones for even parity states. In all panels, calculations have been carried out with a Fock basis truncated at $N = 800$.

as a function of η, for different values of ξ_2', is shown in figures 8(b.1)–(b.4). It is similar to that of the $\hat{P}_2$ term with a two-fold degeneracy in the asymptotic limit of ξ_2' large and requires no further comment.

The spectrum of the Hamiltonian

$$\frac{\hat{H}}{K} = -\eta\hat{n} + \hat{n}\,(\hat{n}-1) - \xi_4\hat{P}_4 \tag{60}$$

is shown in the panels of figure 10 for $\xi_4 = 0.05$. This Hamiltonian is the same that was studied in [8], where a promising quantum error correction scheme was proposed. The spectrum of this Hamiltonian has remarkable new features when compared with that of the $\hat{P}_2$ term in (56) depicted in figure 7(a); the most notable being that, in the asymptotic limit, the eigenstates of the Hamiltonian (60) have four-fold degeneracy. To clarify this situation, we show in figure 10(a) the eigenvalues as a function of η for $\xi_4 = 0.05$, colored by parity. We see here crossings of states both with opposite parity, $\pi = +,-$, and with the same parity, $\pi = +,+$ and $\pi = -,-$, and also avoided crossings of states with the same parity. This property is due to the fact that the $\hat{P}_4$ term couples states with oscillator quantum number n differing by four units, i.e. $n\,\mathrm{mod}\,4$. This property is evinced in figure 10(b), where now the states are colored with $\mathrm{mod}\,4$. In other words, while in figure 10(a) the coloring is that of two copies of the cyclic group $C_2 \equiv \Pi$, in figure 10(b) the coloring is that of the cyclic group, C_4, where C_ν is the cyclic group of order ν. This is a special property of the group C_4, which can be split into $C_2 \oplus C_2$. The spectrum of the Hamiltonian (60) as a function of η for different values of ξ_4 is shown in figure 11, with states in panels (a.1)–(a.4) depicted using the $\mathrm{mod}\,2 \oplus \mathrm{mod}\,2$ coloring scheme and in panels (b.1)–(b.4) using the $\mathrm{mod}\,4$ scheme. Note that this $\hat{P}_4$ Hamiltonian term can be implemented in experiments like those in [9, 10] by further engineering the hardware [57] and driving conditions [8, 34].

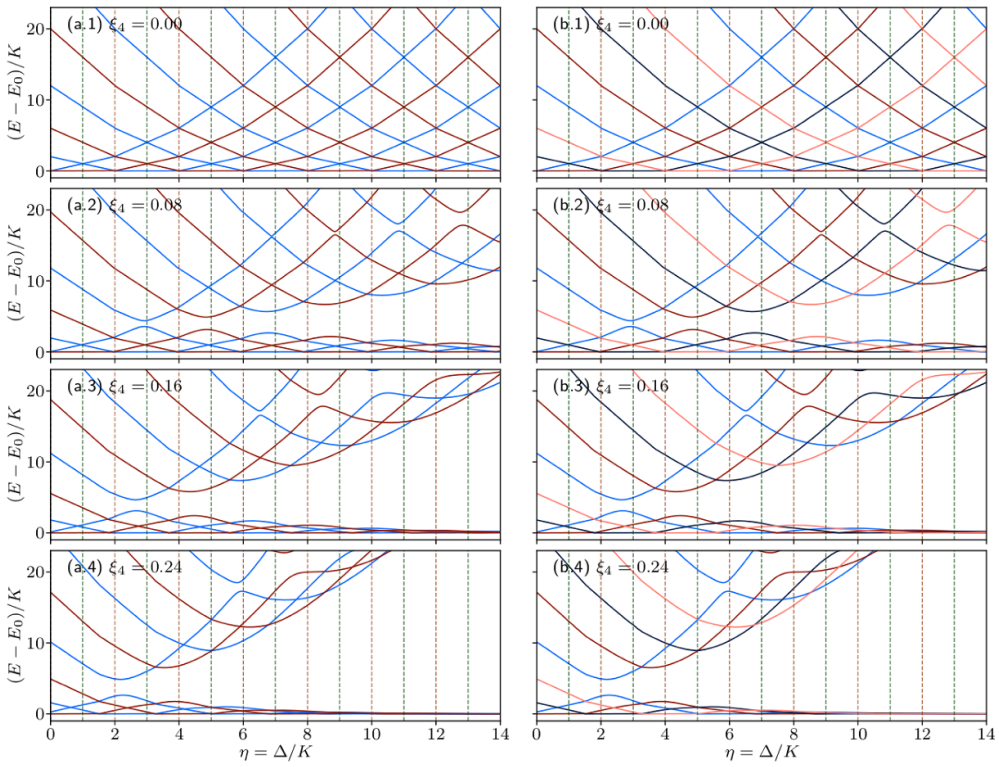

Figure 11. Spectrum of the Hamiltonian (60) as a function of η for different values of ξ_4. Panels (a.1)–(a.4): States identified with a $\mathrm{mod}\,2 \oplus \mathrm{mod}\,2$ coloring. The blue color denotes positive parity states and the red color negative parity states. Panels (b.1)–(b.4): States identified with a $\mathrm{mod}\,4$ coloring scheme. In all panels, calculations have been carried out with a Fock basis truncated at $N = 800$.

For purposes of studying the stability of the solutions of the Hamiltonian (22), it is also of interest to consider the effect of other perturbations, in addition to those contained in the Hamiltonian of section 1. Particularly interesting is the term of order 3, which can be experimentally implemented via the correct driving condition [30, 34],

$$\varepsilon_3 \hat{P}_3 = \varepsilon_3 \left(\hat{a}^{\dagger 3} + \hat{a}^3\right). \tag{61}$$

The spectrum of the Hamiltonian

$$\frac{\hat{H}}{K} = -\eta \hat{n} + \hat{n}\left(\hat{n} - 1\right) - \xi_3 \hat{P}_3 \tag{62}$$

is shown in figure 12 for $\xi_3 = 0.1$ and in figure 13 as a function of η for different values of ξ_3. This spectrum, first studied in [11], has also some remarkable properties, since in the asymptotic limit, the states have a three-fold degeneracy and are representations of the cyclic group C_3. Also, parity here is not a good quantum number, since the $\hat{P}_3$ term couples states with n differing by three units, i.e. $n\,\mathrm{mod}\,3$. The coloring with different shades of green in figures 12 and 13 reflects this property.

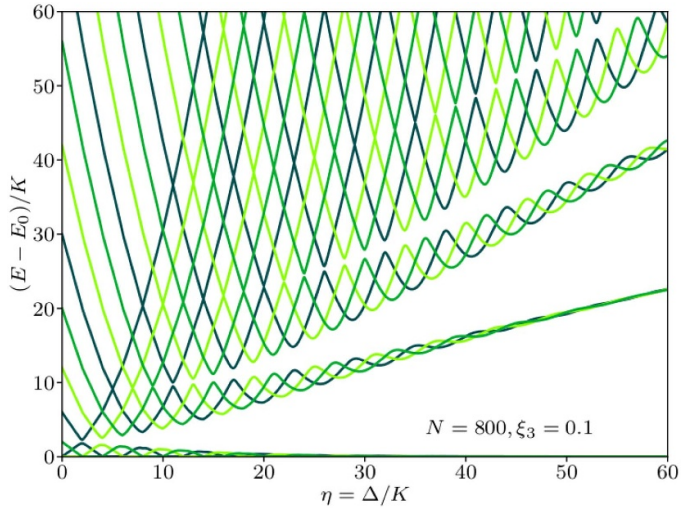

Figure 12. Spectrum of the Hamiltonian (62) for $\xi_3 = 0.1$. The different shades of green denote states within a mod 3 coloring scheme. The Fock space is truncated at $N = 800$.

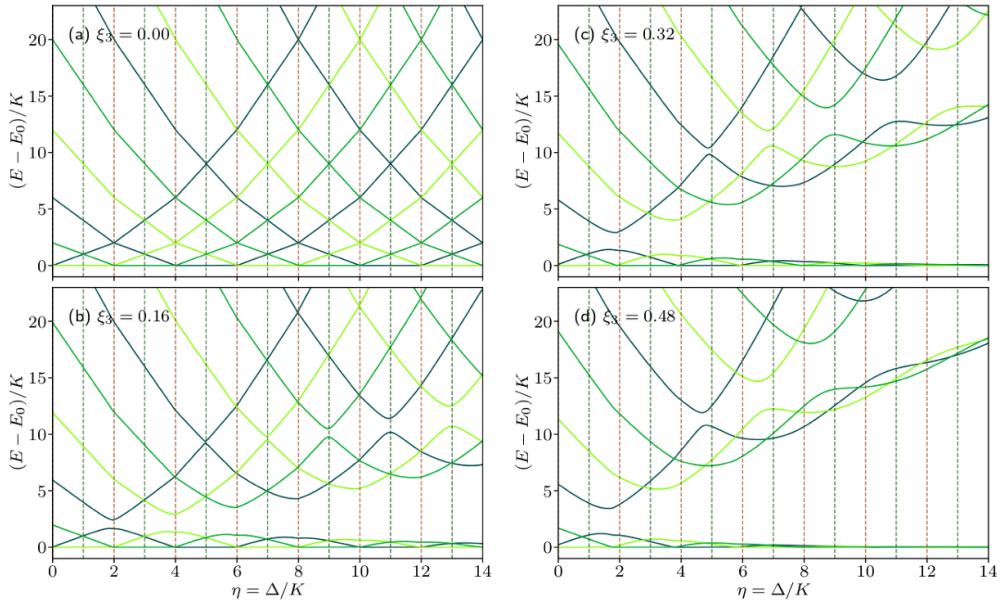

Figure 13. Spectrum of Hamiltonian (62) as a function of η for different values of ξ_3 with a mod 3 coloring scheme. The Fock space is truncated at $N = 800$.

It is remarkable that the quasi-spin symmetry of Hamiltonian (22) is robust for the term $\hat{P}_2$: the value of η remains at even $\eta = 2,4,6,\ldots$ for crossings of states with different parity and at odd $\eta = 1,3,5,\ldots$ for avoided crossings of states with the same parity. For the other terms, the value of η changes and other crossings and avoided crossings occur. The change of the value of η from even $\eta = 0,2,4,6$ as a function of the coupling strength ξ for the perturbations $\hat{P}_2$,

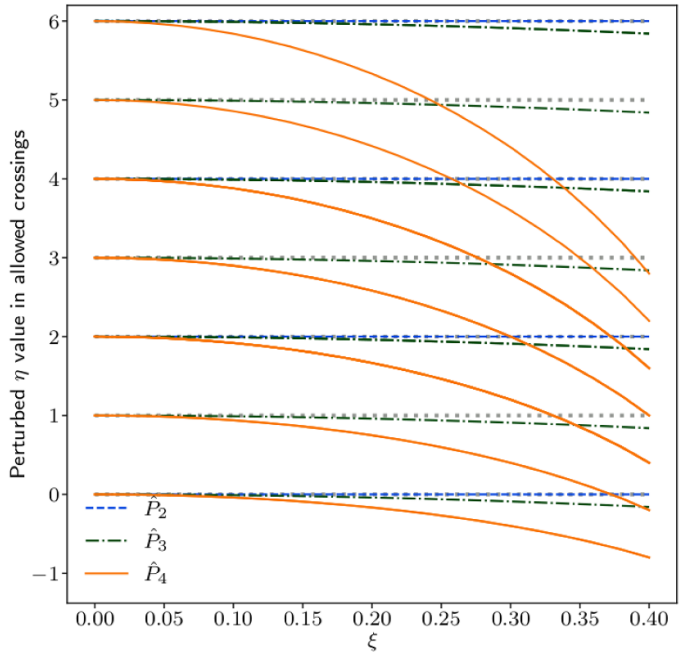

Figure 14. Behavior of the location of the degeneracies $\pm m$ as a function of the strength ξ for the representations $j = 1/2,\ 3/2,\ 5/2$, and $7/2$ ($\eta = 0, 2, 4, 6$) for $\hat{P}_2$, $\hat{P}_3$, and $\hat{P}_4$ and the representations $j = 1, 2$, and 3 ($\eta = 1, 3, 5$) for $\hat{P}_3$ and $\hat{P}_4$.

$\hat{P}_3$, and $\hat{P}_4$ is shown in figure 14. One can see from this figure that for $\hat{P}_2$, no change occurs, even for large (non-perturbative) values of the perturbation strength ξ. The change is small and independent of η for $\hat{P}_3$ and considerably larger and dependent on η for $\hat{P}_4$. As shown in figure 14, the $\hat{P}_3$ and $\hat{P}_4$ perturbations have also allowed crossings for odd η values, with the same dependence than in the even η cases: small and η independent variations in the $\hat{P}_3$ case and larger and η-dependent variations in the $\hat{P}_4$ case. These results have important implications for Hamiltonian stabilization of bosonic codes for quantum information [5, 9, 10].

Another interesting result is that in the asymptotic limit of large coupling ξ, the degeneracies change from the two-fold degeneracy of $\hat{P}_2$ to a three-fold degeneracy in $\hat{P}_3$ and a four-fold degeneracy in $\hat{P}_4$. A full study of the algebraic structure of the $\hat{P}_3$ and $\hat{P}_4$ terms and their associated symmetries remains to be done, especially in relation to their braiding properties shown in figures 10 and 12.

6. Summary and conclusions

In this article, we have investigated the symmetries of the squeeze-driven Kerr oscillator, discovered a hitherto unknown quasi-spin symmetry of the Hamiltonian $\hat{H} = -\Delta\hat{n} + K\hat{n}(\hat{n} - 1)$, and shown that solutions at even values of the ratio $\eta = \Delta$(detuning)/K(Kerr coefficient) are very stable to perturbations induced by the ratio $\xi = \varepsilon_2$(squeezing amplitude)/K(Kerr coefficient), and moderately stable to perturbations induced by high order terms in the boson expansion of the Hamiltonian. This result has major implications for the use of the squeeze-driven Kerr oscillator in quantum computing. In particular, the discovery of the quasi-spin

symmetry of the Kerr-Hamiltonian may have major implications when going from a KPO (Kerr Parametric Oscillator) to an OPO (Open Parametric Oscillator), that is from the solutions of the Hamiltonian operator to the solutions of the Limbladian operator. Work on the study of symmetries of Limbladian operators by one of the authors (F.I.) and J. Venkatraman is in progress.

The study of the symmetry $su(2)$ of the Kerr oscillator presented here can be extended to two coupled Kerr oscillators $su(2)_1 \oplus su(2)_2$ in the same way in which it is done in the proton-neutron interacting boson model (IBM2) in nuclear physics $su(6)_1 \oplus su(6)_2$ [42], in triatomic molecules $su(4)_1 \oplus su(4)_2$ [43], and coupled benders $su(3)_1 \oplus su(3)_2$ [58] in molecular physics, and, most importantly, to a large number of coupled oscillators $\sum_i \oplus su(2)_i$ on a lattice, in the same way in which it is done in the algebraic theory of crystal vibrations [59, 60], for example in an Ising lattice [2, 7, 14, 31, 61], thus playing an important role in the development of quantum computers based on Kerr parametric oscillators [2, 4], which is the ultimate goal of the research initiated in this article. The study of the symmetries of two squeeze-driven Kerr oscillators requires a generalization of the methods of [42, 43] to their non-compact versions, in particular, for the one-dimensional squeeze-driven Kerr oscillator to the coupled algebras $sp(2,\mathbb{R})_1 \oplus sp(2,\mathbb{R})_2$. This study, however, is relatively straightforward, since the algebra of $sp(2,\mathbb{R})$ is isomorphic to $su(1,1)$, the non-compact version of the familiar angular momentum algebra. Generalization to nonlinear parametric oscillators with quartic terms $\hat{a}^{\dagger 4}\hat{a}^4$ or higher nonlinearities are also possible by expanding the symmetry from $su(2)$ to $su(4)$ or $su(n)$.

Further applications of the group-theoretic methods and techniques discussed in this paper are to the study of squeeze-driven systems other than the Kerr oscillator, and to their associated quantum phase transitions (QPT) and excited state quantum phase transitions (ESQPT), for example to the squeeze-driven Rabi and Dicke models [38, 39] and the Jaynes–Cummings model [38]. The algebraic structure of these models is that of $sp(2,\mathbb{R})$ generated by $\hat{a}^\dagger\hat{a}, \hat{a}^{\dagger 2}, \hat{a}^2$ coupled to $su(2)$ generated by $\sigma_x, \sigma_y, \sigma_z$, that is $sp(2,R) \oplus su(2)$.

Data availability statement

The data that support the findings of this study are openly available at the following URL/DOI: https://gitlab.com/currix1/symmetries-of-the-squeeze-driven-kerr-oscillator.

Acknowledgments

This research was supported by the NSF CCI Grant (Award Number 2124511). R G C acknowledges discussions with J Venkatraman, X Xiao, M Devoret, and P and V Kurilovich. F P B thanks funding received from the European Union's Horizon 2020 research and innovation program under the Marie Skłodowska-Curie Grant Agreement No 872081 and from Grant PID2019-104002GB-C21 funded by MCIN/AEI/ 10.13039/501100011033 and, as appropriate, by 'ERDF A way of making Europe', by the 'European Union' or by the 'European Union NextGenerationEU/PRTR'. Computing resources supporting this work were partially provided by the CEAFMC and Universidad de Huelva High Performance Computer (HPC@UHU) located in the Campus Universitario el Carmen and funded by FEDER/MINECO Project UNHU-15CE-2848.

ORCID iDs

Rodrigo G Cortiñas https://orcid.org/0000-0002-3706-306X

Francisco Pérez-Bernal https://orcid.org/0000-0002-3009-3696
Lea F Santos https://orcid.org/0000-0001-9400-2709

References

[1] Goto H 2016 Bifurcation-based adiabatic quantum computation with a nonlinear oscillator network *Sci. Rep.* **6** 21686
[2] Goto H 2019 Quantum computation based on quantum adiabatic bifurcations of Kerr-nonlinear parametric oscillators *J. Phys. Soc. Japan* **88** 061015
[3] Mirrahimi M, Leghtas Z, Albert V V, Touzard S, Schoelkopf R J, Jiang L and Devoret M H 2014 Dynamically protected cat-qubits: a new paradigm for universal quantum computation *New J. Phys.* **16** 045014
[4] Puri S, Boutin S and Blais A 2017 Engineering the quantum states of light in a Kerr-nonlinear resonator by two-photon driving *npj Quantum Inf.* **3** 1–7
[5] Grimm A, Frattini N E, Puri S, Mundhada S O, Touzard S, Mirrahimi M, Girvin S M, Shankar S and Devoret M H 2020 Stabilization and operation of a Kerr-cat qubit *Nature* **584** 205–9
[6] Blais A, Grimsmo A L, Girvin S M and Wallraff A 2021 Circuit quantum electrodynamics *Rev. Mod. Phys.* **93** 025005
[7] Darmawan A S, Brown B J, Grimsmo A L, Tuckett D K and Puri S 2021 Practical quantum error correction with the XZZX code and Kerr-cat qubits *PRX Quantum* **2** 030345
[8] Kwon S, Watabe S and Tsai J-S 2022 Autonomous quantum error correction in a four-photon Kerr parametric oscillator *npj Quantum Inf.* **8** 40
[9] Frattini N E *et al* 2022 The squeezed Kerr oscillator: spectral kissing and phase-flip robustness (arXiv:2209.03934)
[10] Venkatraman J, Cortinas R G, Frattini N E, Xiao X and Devoret M H 2022 A driven quantum superconducting circuit with multiple tunable degeneracies (arXiv:2211.04605)
[11] Venkatraman J 2023 Controlling the effective Hamiltonian of a driven quantum superconducting circuit *PhD Thesis* Yale University (available at: www.proquest.com/openview/fd652ab459a37d707aa0fc9f15905927/1?pq-origsite=gscholar&cbl=18750&diss=y)
[12] Kirchmair G, Vlastakis B, Leghtas Z, Nigg S E, Paik H, Ginossar E, Mirrahimi M, Frunzio L, Girvin S M and Schoelkopf R J 2013 Observation of quantum state collapse and revival due to the single-photon Kerr effect *Nature* **495** 205–9
[13] Rehák M, Neilinger P, Grajcar M, Oelsner G, Hübner U, Il'ichev E and Meyer H-G 2014 Parametric amplification by coupled flux qubits *Appl. Phys. Lett.* **104** 162604
[14] Puri S, Andersen C K, Grimsmo A L and Blais A 2017 Quantum annealing with all-to-all connected nonlinear oscillators *Nat. Commun.* **8** 15785
[15] Goto H, Lin Z and Nakamura Y 2018 Boltzmann sampling from the Ising model using quantum heating of coupled nonlinear oscillators *Sci. Rep.* **8** 7154
[16] Amin M H, Andriyash E, Rolfe J, Kulchytskyy B and Melko R 2018 Quantum Boltzmann machine *Phys. Rev.* X **8** 021050
[17] Yamamoto T, Inomata K, Watanabe M, Matsuba K, Miyazaki T, Oliver W D, Nakamura Y and Tsai J S 2008 Flux-driven Josephson parametric amplifier *Appl. Phys. Lett.* **93** 042510
[18] Bourassa J, Beaudoin F, Gambetta J M and Blais A 2012 Josephson-junction-embedded transmission-line resonators: from Kerr medium to in-line transmon *Phys. Rev.* A **86** 013814
[19] Wustmann W and Shumeiko V 2013 Parametric resonance in tunable superconducting cavities *Phys. Rev.* B **87** 184501
[20] Krantz P, Reshitnyk Y, Wustmann W, Bylander J, Gustavsson S, Oliver W D, Duty T, Shumeiko V and Delsing P 2013 Investigation of nonlinear effects in Josephson parametric oscillators used in circuit quantum electrodynamics *New J. Phys.* **15** 105002
[21] Eichler C and Wallraff A 2014 Controlling the dynamic range of a Josephson parametric amplifier *EPJ Quantum Technol.* **1** 2
[22] Lin Z R, Inomata K, Koshino K, Oliver W D, Nakamura Y, Tsai J S and Yamamoto T 2014 Josephson parametric phase-locked oscillator and its application to dispersive readout of superconducting qubits *Nat. Commun.* **5** 4480
[23] Krantz P, Bengtsson A, Simoen M, Gustavsson S, Shumeiko V, Oliver W D, Wilson C M, Delsing P and Bylander J 2016 Single-shot read-out of a superconducting qubit using a Josephson parametric oscillator *Nat. Commun.* **7** 11417

[24] Dykman M I and Smelyanski V N 1990 Fluctuational transitions between stable states of a nonlinear oscillator driven by random resonant force *Phys. Rev.* A **41** 3090–102
[25] Marthaler M and Dykman M I 2007 Quantum interference in the classically forbidden region: a parametric oscillator *Phys. Rev.* A **76** 010102
[26] Dykman M 2012 *Fluctuating Nonlinear Oscillators from Nanomechanics to Quantum Superconducting Circuits* vol 07 (Oxford University Press)
[27] Peano V, Marthaler M and Dykman M I 2012 Sharp tunneling peaks in a parametric oscillator: quantum resonances missing in the rotating wave approximation *Phys. Rev. Lett.* **109** 090401
[28] Lin Z R, Nakamura Y and Dykman M I 2015 Critical fluctuations and the rates of interstate switching near the excitation threshold of a quantum parametric oscillator *Phys. Rev.* E **92** 022105
[29] Goto H 2016 Universal quantum computation with a nonlinear oscillator network *Phys. Rev.* A **93** 050301
[30] Zhang Y and Dykman M I 2017 Preparing quasienergy states on demand: a parametric oscillator *Phys. Rev.* A **95** 053841
[31] Dykman M I, Bruder C, Lörch N and Zhang Y 2018 Interaction-induced time-symmetry breaking in driven quantum oscillators *Phys. Rev.* B **98** 195444
[32] Roberts D and Clerk A A 2020 Driven-dissipative quantum Kerr resonators: new exact solutions, photon blockade and quantum bistability *Phys. Rev.* X **10** 021022
[33] Venkatraman J, Xiao X, Corti nas R G, Eickbusch A and Devoret M H 2022 Static effective Hamiltonian of a rapidly driven nonlinear system *Phys. Rev. Lett.* **129** 100601
[34] Xiao X, Venkatraman J, Cortiñas R G, Chowdhury S and Devoret M H 2023 A diagrammatic method to compute the effective Hamiltonian of driven nonlinear oscillators (arXiv:2304.13656)
[35] García-Mata I, Cortiñas R G, Xiao X, Chávez-Carlos J, Batista V S, Santos L F and Wisniacki D A 2023 Effective versus Floquet theory for the Kerr parametric oscillator (arXiv:2309.12516)
[36] Prado Reynoso M A, Nader D J, Chávez-Carlos J, Ordaz-Mendoza B E, Corti nas R G, Batista V S, Lerma-Hernández S, Pérez-Bernal F and Santos L F 2023 Quantum tunneling and level crossings in the squeeze-driven Kerr oscillator *Phys. Rev.* A **108** 033709
[37] Chávez-Carlos J, Lezama T L M, Cortiñas R G, Venkatraman J, Devoret M H, Batista V S, Pérez-Bernal F and Santos L F 2023 Spectral kissing and its dynamical consequences in the squeeze-driven Kerr oscillator *npj Quantum Inf.* **9** 76
[38] Shen Li-T, Tang C-Q, Shi Z, Wu H, Yang Z-B and Zheng S-B 2022 Squeezed-light-induced quantum phase transition in the jaynes-cummings model *Phys. Rev.* A **106** 023705
[39] Yang J, Shi Z, Yang Z-B, Shen L T and Zheng S-B 2023 First-order quantum phase transition in the squeezed Rabi model *Phys. Scr.* **98** 045107
[40] Ruiz D, Gautier R, Guillaud J and Mirrahimi M 2023 Two-photon driven Kerr quantum oscillator with multiple spectral degeneracies *Phys. Rev.* A **107** 042407
[41] Iachello F 1994 Lie algebras, cohomologies and new applications of quantum mechanics *Contemporary Mathematics* vol 160 (American Mathematical Society) pp 151–71
[42] Iachello F and Arima A 1987 *The Interacting Boson Model* (Cambridge University Press) (https://doi.org/10.1017/CBO9780511895517)
[43] Iachello F and Levine R D 1995 *Algebraic Theory of Molecules* (*Topics in Physical Chemistry*) (Oxford University Press)
[44] Iachello F 2006 *Lie Algebras and Applications* (*Lectures Notes in Physics* vol 708) (Springer) (https://doi.org/10.1007/978-3-662-44494-8)
[45] Braak D 2011 Integrability of the Rabi model *Phys. Rev. Lett.* **107** 100401
[46] Albert V V and Jiang L 2014 Symmetries and conserved quantities in Lindblad master equations *Phys. Rev.* A **89** 022118
[47] Caprio M S, Cejnar P and Iachello F 2008 Excited state quantum phase transitions in many-body systems *Ann. Phys., NY* **323** 1106–35
[48] Cejnar P and Stránský P 2008 Impact of quantum phase transitions on excited-level dynamics *Phys. Rev.* E **78** 031130
[49] Cejnar P, Stránský P, Macek M and Kloc M 2021 Excited-state quantum phase transitions *J. Phys. A: Math. Theor.* **54** 133001
[50] Gilmore R 1974 *Lie Groups, Lie Algebras and Some of their Applications* (Wiley)
[51] van Roosmalen O S 1982 Algebraic description of nuclear and molecular rotation-vibration spectra *PhD Thesis* University of Groningen
[52] Lipkin H J, Meshkov N and Glick A J 1965 Validity of many-body approximation methods for a solvable model *Nucl. Phys.* **62** 188–98

[53] Wybourne B G 1974 *Classical Groups for Physicists* (Wiley)
[54] Heiss W D, Scholtz F G and Geyer H B 2005 The large N behaviour of the Lipkin model and exceptional points *J. Phys. A: Math. Gen.* **38** 1843–51
[55] Santos L F, Távora M and Pérez-Bernal F 2016 Excited-state quantum phase transitions in many-body systems with infinite-range interaction: localization, dynamics and bifurcation *Phys. Rev.* A **94** 012113
[56] Nader D J, González-Rodríguez C A and Lerma-Hernández S 2021 Avoided crossings and dynamical tunneling close to excited-state quantum phase transitions *Phys. Rev.* E **104** 064116
[57] Miano A, Joshi V R, Liu G, Dai W, Parakh P D, Frunzio L and Devoret M H 2023 Hamiltonian extrema of an arbitrary flux-biased Josephson circuit (arXiv:2302.03155)
[58] Larese D, Caprio M A, Pérez-Bernal F and Iachello F 2014 A study of the bending motion in tetratomic molecules by the algebraic operator expansion method *J. Chem. Phys.* **140** 014304
[59] Iachello F, Dietz B, Miski-Oglu M and Richter A 2015 Algebraic theory of crystal vibrations: Singularities and zeros in vibrations of one- and two-dimensional lattices *Phys. Rev.* B **91** 214307
[60] Dietz B, Iachello F and Macek M 2017 Algebraic theory of crystal vibrations: localization properties of wave functions in two-dimensional lattices *Crystals* **7** 246
[61] Kanao T and Goto H 2021 High-accuracy Ising machine using Kerr-nonlinear parametric oscillators with local four-body interactions *npj Quantum Inf.* **7** 18